Journal of Cleaner Production 362 (2022) 132525

Contents lists available at ScienceDirect

Journal of Cleaner Production

journal homepage: www.elsevier.com/locate/jclepro

Surface modification of coal tailings by thermal air oxidation for ammonia capture

Wei Zhang [a], Bing Han [a], Uta Wille [b], Clayton Butterly [a], Ji-Zheng He [a], Deli Chen [a,*]

[a] School of Agriculture and Food, Faculty of Veterinary and Agricultural Sciences, The University of Melbourne, Parkville, Victoria, 3010, Australia
[b] School of Chemistry, Bio21 Institute, The University of Melbourne, Parkville, Victoria, 3010, Australia

ARTICLE INFO

Handling Editor: M.T. Moreira

Keywords:
Adsorption
Ammonia mitigation
Environmental remediation
Mechanism
Nutrient removal
Waste management

ABSTRACT

Utilization of coal tailings (CTs) to enable ammonia (NH_3) capture is of interest from pollution control and waste management perspectives. In this work, CTs were surface modified by air oxidation at different temperatures and varying duration to increase the uptake of NH_3. The CTs treated at 300 and 250 °C for 5 h achieved an NH_3 uptake of 52.5 and 45.3 mg g^{-1}, respectively, which was significantly higher than that of the untreated CT (2.1 mg g^{-1}). A linear relationship between NH_3 uptake and concentration of acidic surface functional groups was found ($R^2 = 0.99$). Spectroscopic analysis showed that NH_3 can be retained on the oxidized CT through chemisorption involving carboxylic groups, leading to the formation of amides. Kinetic studies in the temperature range of 200–300 °C revealed an activation energy of 50.2 kJ mol^{-1} for the formation of acidic surface functional groups on CTs. These comparably mild conditions for the oxidative surface modification make CTs versatile and readily available materials for reducing agricultural NH_3 emissions.

1. Introduction

Ammonia (NH_3) emissions have widespread adverse impacts on the environment and human health. Ammonia in the atmosphere is not only an odour concern (Guffanti et al., 2018), but also contributes to the formation of particulate matter with aerodynamic diameters $\leq$2.5 μm ($PM_{2.5}$) (Gu et al., 2021). Atmospheric NH_3 deposited on land surfaces can ultimately lead to emissions of the greenhouse gas nitrous oxide (N_2O) (Petersen, 2018), soil acidification, water eutrophication, and loss of biodiversity (Sutton et al., 2011). Agricultural activities such as the use of synthetic nitrogen (N) fertilizer and livestock production are responsible for up to 90% of total NH_3 emissions globally (Xu et al., 2019; Beusen et al., 2008). In particular, the decomposition of urea (in mammals) or uric acid (in birds) in livestock manure can release large amounts of NH_3 into the atmosphere. On the other hand, the highly energy-intensive Haber-Bosch process for NH_3 synthesis and industrial fertilizer production consumes 1–2% of the annual global energy supply (Nancharaiah et al., 2016). Given that fertilizer demand and livestock production are expected to steeply increase in the coming decades in response to agricultural intensification to feed the growing population, conserving and utilizing N nutrient from livestock manure has economic and environmental benefits (Zhang et al., 2020b; Stokstad, 2014).

Manure additives can be used to reduce NH_3 emissions from intensive livestock operations and retain the valuable N nutrient in manure. The most commonly employed manure additives are acidifying agents that suppress NH_3 volatilization by lowering manure pH (McIlroy et al., 2019), urease inhibitors that slow down the microbiological hydrolysis of manure urea to ammonium (NH_4^+) (Bobrowski et al., 2021; Hagenkamp-Korth et al., 2015), and adsorbents with a high affinity for NH_4^+ (Wang et al., 2012). However, acidifying additives, such as sulfuric, hydrochloric and nitric acids, are not only corrosive and hazardous, but could also lead to an undesirable increase of the manure mineral content. On the other hand, urease inhibitors, such as *N*-(*n*-butyl)thiophosphoric triaminde (NBPT), are prone to hydrolysis and require frequent applications to remain efficient. Although adsorbent materials, such as zeolites, could be easily implemented in livestock farms, so far, they have only been investigated under laboratory conditions. Our group for the first time reported that application of lignite (i.e., brown coal) to cattle pens reduced NH_3 emissions from cattle feedlots by 66% (Chen et al., 2015). Lignite has rich pore structures, high concentrations of surface functionalities and a low pH, which makes it an effective adsorbent material for NH_3 (Han et al., 2021). However, the

* Corresponding author.
E-mail addresses: zhangw13@student.unimelb.edu.au (W. Zhang), bing.han@unimelb.edu.au (B. Han), uwille@unimelb.edu.au (U. Wille), clayton.butterly@unimelb.edu.au (C. Butterly), jizheng.he@unimelb.edu.au (J.-Z. He), delichen@unimelb.edu.au (D. Chen).

https://doi.org/10.1016/j.jclepro.2022.132525
Received 28 December 2021; Received in revised form 27 May 2022; Accepted 30 May 2022
Available online 1 June 2022

considerable weight of lignite due to its high moisture content (up to 70%) makes transport to distant livestock farms uneconomical, which has negative impacts on the environment (Ng et al., 2020). Therefore, if coal mining wastes could be surface-modified to enhance NH_3 capture, a readily available alternative to lignite could be used in livestock farms for mitigation of manure NH_3 emissions.

Coal tailings (CTs) are fine (<2 mm diameter) wastes from the coal washing process, which typically consist of fine coal particles and gangue mineral matter such as clays (aluminosilicates) and quartz (silicates) (Tremain et al., 2014). Handling large volumes of CTs is one of the major challenges the coal industry is facing. Approximately 10% of run-of-mine coal production is disposed of as tailings that are conventionally pumped as an aqueous slurry to tailings dams (Radloff et al., 2004), causing environmental and safety risks such as windblown dust, water contamination, acid drainage and dam structure failure to mining companies and surrounding communities (Santamarina et al., 2019; Edraki et al., 2014). Therefore, the exploration of alternative uses of CTs to eliminate these environmental and health hazards is an active area of research. Furthermore, the proposed usage of CTs to capture agricultural NH_3 has the potential to serve as a new source of revenue for mining companies and a new waste management strategy for both mining companies and livestock farms. Although activated carbon is the most widely used carbon adsorbent owing to its porous structure and large surface area, unfortunately, NH_3 adsorption capacities of commercial activated carbons are very small (e.g., 0.15–5.3 mg g^{-1}) (Goncalves et al., 2011; Huang et al., 2008; Le Leuch and Bandosz, 2007). Previous studies have revealed that acidic functionalities on surfaces of carbonaceous materials play an important role for the adsorption of NH_3 (Mochizuki et al., 2016; Zheng et al., 2016; Huang et al., 2008). Apart from oxidation using gaseous and aqueous oxidants, such as strong mineral acids, ozone and plasma treatments, which are hazardous or require specialized equipment (Rehman et al., 2019), it has been recently demonstrated that thermal air oxidation provides a simple, environmentally benign and non-hazardous strategy to introduce acidic functionalities on surfaces of black coal with high efficiency to increase the NH_3 capture capacity (Zhang et al., 2020a). However, the adsorption mechanisms of NH_3 and the reaction kinetics of formation of acidic surface functional groups during thermal air oxidation are not well understood.

In the present study, we have therefore explored surface-modified CTs by: (i) investigating the effects of air oxidation temperature and time on the uptake of gaseous NH_3 and aqueous NH_4^+; (ii) identifying the adsorption sites and probable mechanisms involved; and (iii) studying the reaction kinetics for the formation of acidic surface functional groups on CTs.

2. Materials and methods

2.1. Thermal air oxidation of coal tailings

The CTs were sourced as a slurry from a coal mine in New South Wales (NSW), Australia, and were concentrated by decanting the supernatant liquid to increase the solid percentage by mass to approximately 60%. The CTs were filled into aluminium containers (internal diameter 80 mm, height 36 mm) to a height of approximately 15 mm and heated in a forced air-drying oven (Across International, model FO-19070) at temperatures varied in 50 °C increments between 150 and 400 °C. The effect of oxidation time on the extent of surface modification was investigated at 250 °C by removing containers from the oven after 1, 2, 3, 4, 5 6 and 7 h, followed by grinding with a mortar and pestle to ensure homogeneity. The sample nomenclature was assigned as CT, followed by the time (hours) and temperature (°C) of air oxidation. For example, the samples obtained at 250 °C for 5 and 7 h were denoted as CT-5-250 and CT-7-250, respectively.

2.2. Chemical characterization of coal tailings

The concentrated CTs (by decanting the supernatant liquid) were oven dried at 70 °C until a constant weight was reached, followed by grinding with a mortar and pestle. Elemental analysis was carried out in accordance with the Australian Standard Methods (AS 1038.3). Total carbon (C) and total N were analysed by dry combustion with an elemental analyser (TruMac CN, LECO). Total oxygen (O) was determined by pyrolysis, and total hydrogen (H) was determined by combustion with a FlashSmart Elemental Analyser (Thermo-Scientific). Total sulphur (S) was determined by infrared method (AS 1038.6.3.3). Mercury (Hg), antimony (Sb), selenium (Se) and boron (B) were determined using the acid digestion method with atomic absorption spectrometric (AAS, GBC SavantAA) and inductively coupled plasma optical emission spectroscopy (ICP-OES, SPECTRO ARCOS) analyses (AS 1038.10.5.2). The other major, minor and trace elements were determined in CT ash using the acid digestion method with ICP-OES analysis (AS 1038.10). Thermogravimetric (TG) analysis was undertaken using a thermogravimetric analyser (TGA 8000, PerkinElmer) by heating about 10 mg sample from 40 to 800 °C at a heating rate of 5 °C min^{-1} under an air stream of 30 mL min^{-1}. The Brunauer–Emmett–Teller (BET) surface area (S_{BET}) and total pore volume (V_{total}) were determined after vacuum degassing the sample for 24 h at 70 °C on a Micromeritics instrument (ASAP, 2020) by fitting the amount of N_2 adsorbed at −196 °C (Sumaraj et al., 2020). Pore size distribution was obtained from application of Barrett-Joyner-Halenda (BJH) method assuming Harkins-Jura's (HJ) equation on the N_2 adsorption isotherm. Scanning electron microscopy (SEM) images were performed on a sample powder without coating at an accelerating voltage of 20 kV using a FlexSEM 1000.

Evaluation of the chemical changes in CTs following thermal air oxidation was performed by measuring pH and surface oxygen-containing functional groups using diffuse reflectance infrared Fourier transform (DRIFT) spectroscopy, X-ray photoelectron spectroscopy (XPS) and the Boehm titration method. The pH was measured after shaking a 1:10 (1 g in 10 mL) suspension of sample in reverse osmosis water overnight. DRIFT spectra in the range of 400–4000 cm^{-1} with a resolution of 4 cm^{-1} were obtained using a Frontier Optica FT-IR spectrometer (PerkinElmer) fitted with an AutoDiff II diffuse reflectance autosampler (PIKE Technologies). XPS spectra were obtained using a Kratos Axis Ultra XPS (Thermo Fisher Scientific, UK) under severe vacuum pressure (1.3×10^{-6} Pa) with A1 Kα radiation and a fixed photon energy of 1486.6 eV. In addition to a broad survey scan in the range of 0–1200 eV with a resolution of 1.0 eV, high-resolution scans for C 1s (282–294 eV), N 1s (396–408 eV) and O 1s (529–537 eV) were conducted with a resolution of 0.05 eV. Data analysis and curve fitting were performed using CasaXPS software (version 2.3.19PR1.0), and the binding energies of C 1s in survey scan and C–C bond in high resolution scan were calibrated at 285.0 eV (Sumaraj et al., 2020). The concentration of acidic surface functional groups on CTs was determined by the Boehm titration method (Goertzen et al., 2010). Briefly, 1.0 g of sample was mixed with 50 mL of either aqueous sodium bicarbonate ($NaHCO_3$), sodium carbonate (Na_2CO_3), or sodium hydroxide (NaOH) (0.05 N solutions in each case). The mixtures were shaken for 24 h, filtered (0.45 μm), and 20 mL of each filtrate was directly titrated with hydrochloric acid (HCl, 0.05 N). The concentration of each type of acidic functional groups per gram of sample (mmol g^{-1}) was calculated under the assumption that $NaHCO_3$ neutralized strong acidic groups (mainly carboxylic groups); Na_2CO_3 neutralized strong and moderate acidic groups (mainly lactones, which are included as they form acids upon hydrolysis); and NaOH neutralized all types of acidic groups, including strong, moderate, and weak acidic groups (mainly phenols).

2.3. Determination of the NH_3 and NH_4^+ uptake

Determination of the NH_3 and NH_4^+ uptake was carried out at room temperature (23.0 ± 0.3 °C) in a temperature-controlled lab. NH_3

uptake was determined using a gravimetric method by exposing 1.0 g of each sample to NH_3 gas released from a 25% aqueous NH_3 solution at ambient pressure. The amount of NH_3 captured by the sample was gravimetrically recorded as a function of time using the microbalance. The measurements were performed in triplicate and NH_3 uptake was determined from the weight gain of the sample after 60 min gas exposure. Control experiments, where the sample was exposed to water under otherwise identical conditions, were performed to determine the uptake of water and to correct the data from the exposure to NH_3 gas released from the aqueous NH_3 solution.

NH_4^+ uptake was determined using a batch method by mixing 1.0 g of each sample with 50 mL of an aqueous ammonium chloride solution (NH_4Cl, 500 mg L^{-1}). The concentration of the NH_4Cl solution chosen was based on the NH_4^+-N concentration of 104–338 mg kg^{-1} measured in cattle manure in feedlot pen surfaces (Sun et al., 2016). All samples were then shaken for 24 h at room temperature, followed by centrifuging and filtering (Whatman #1). The NH_4^+ concentration in the supernatant was measured by a continuous flow analyser (San++, Skalar), and the amount of NH_4^+ taken up by the sample was calculated from the difference between the NH_4^+ concentration in the initial solution and in the supernatant. The percentage removal efficiency (%) of NH_4^+ from the aqueous solution was calculated as the amount of NH_4^+ removed compared to the initial NH_4^+. All chemicals used in this study were analytical reagent grade and Milli-Q water was used throughout the experiment.

3. Results and discussion

3.1. Characterization of coal tailings

The untreated CT had a high ash content of 44.4% and significant quantities of silicon (Si, 13.5%) and aluminium (Al, 8.0%), indicating a high level of mineral matter such as silica and aluminosilicate (Tremain et al., 2014), whereas the sulphur content (S, 0.4%) was very low (Table 1). The TG analysis of the untreated CT revealed a slight decrease of 0.7% in weight at a temperature below 104.4 °C due to the evaporation of moisture (Fig. 1). The weight then slightly increased by 1.1% with increasing temperature (up to 322.6 °C), which could be caused by the incorporation of oxygen (O) into CTs through the reaction of coal with O_2 leading to the formation of labile O–O functionalities (e.g., peroxides and hydroperoxides) as well as more stable phenolic, carbonyl and carboxyl groups (Zhang et al., 2017; Wang et al., 2003). Further increase in temperature resulted in a rapid decrease of weight due to coal combustion, with a maximum weight loss rate peak point at 558.5 °C on the DTG curve. These results suggest that air oxidation should be performed at temperatures <322.6 °C to achieve the desired CT surface functionalization.

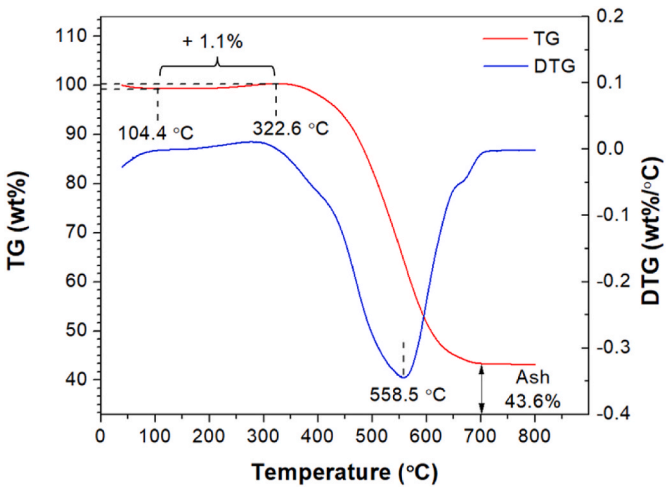

Fig. 1. Thermogravimetric (TG, red line) analysis of the untreated coal tailing for weight loss as a function of temperature and derivative thermogravimetric (DTG, blue line) curve.

3.2. Improvements of surface functionalities

The pH of an aqueous suspension of CTs was used as an indicator for the degree of surface oxidation and formation of acidic functional groups. While the untreated CT was alkaline (pH = 10.0), increasing the oxidation temperature to 250 and 300 °C resulted in a drop of the pH to 6.4 (Fig. 2a). However, at higher temperatures the pH increased to values > 7, possibly due to the thermal decomposition of less stable acidic surface functionalities (Vivo-Vilches et al., 2014). Keeping the oxidation temperature at 250 °C revealed a continual decrease of the pH upon increase of the oxidation time from 1 to 7 h (Fig. 2b). It should be also noted that the pH can be lowered to 7.4 even only after 1 h of treatment (at 250 °C), showing that thermal air oxidation is a rapid and effective way to alter the surface and chemical properties of CTs.

The concentrations of strong, moderate and weak acidic functional groups (mainly carboxylic groups, lactones and phenols, respectively)

Table 1
Composition of the untreated coal tailing (CT) and an exemplary CT sample exposed to thermal air oxidation (CT-5-250).

Proximate analysis (%)	Volatile matter	Fixed carbon	Ash						
Untreated CT	17.4	38.2	44.4						
Oxidized CT	18.2	36.8	45.0						
Elemental analysis (%)	C	N	O	H	S				
Untreated CT	39.5	1.1	8.7	2.9	0.4				
Oxidized CT	40.1	1.1	14.7	2.0	0.4				
Major elements (%)	Si	Al	Fe	Ti	P	Ca	Mg	Na	K
Untreated CT	13.5	8.0	1.4	0.3	0.1	1.3	0.4	0.3	0.8
Oxidized CT	14.6	8.5	1.4	0.3	0.1	1.2	0.4	0.3	0.8
Trace elements (mg kg^{-1})	Cr	Cu	Hg	Mn	Ni	As	Pb	Zn	Cd
Untreated CT	20.7	35.5	0.2	115	13.5	3.5	12.1	25.5	<0.1
Oxidized CT	19.7	32.3	0.1	95.2	13.0	3.0	11.4	25.3	<0.1
Porous characteristics[a]	S_{BET}[b] (m^2 g^{-1})	V_{total}[c] (cm^3 g^{-1})							
Untreated CT	6.8	0.013							
Oxidized CT	5.3	0.013							

[a] Pore size distribution (Fig. S1 in the SI) was obtained from application of Barrett-Joyner-Halenda (BJH) method assuming Harkins-Jura's (HJ) equation.
[b] Specific surface area was determined by the Brunauer–Emmett–Teller (BET) method.
[c] Single point adsorption total pore volume.

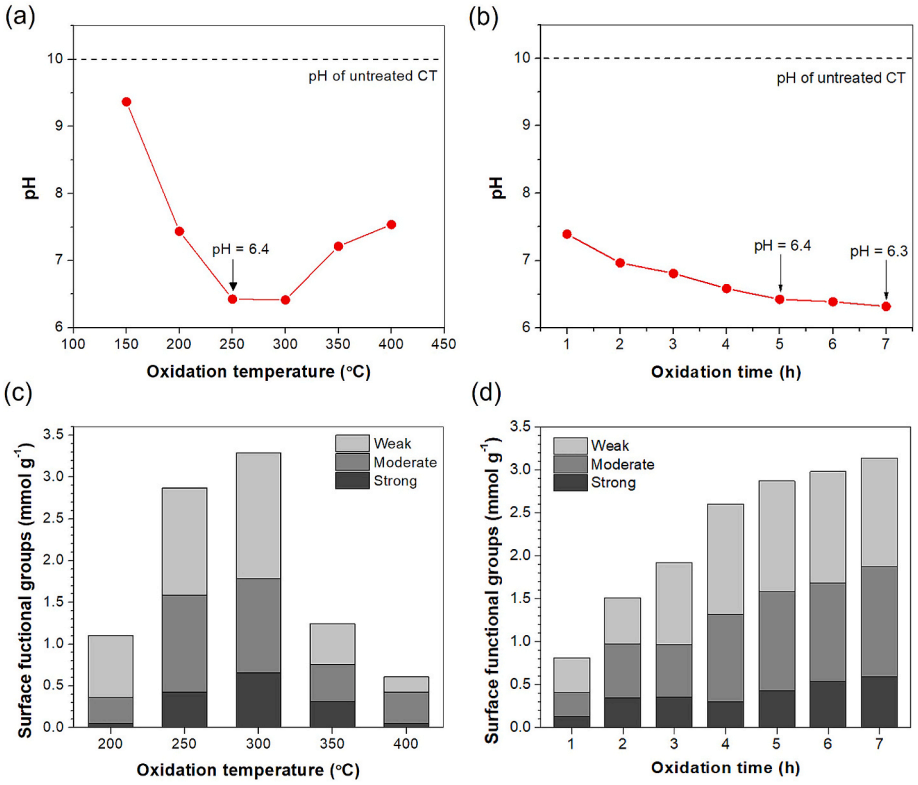

Fig. 2. pH and concentration of acidic surface functional groups (strong, moderate, and weak acidic groups) of oxidized coal tailings (CTs) determined by Boehm titration: effect of (a, c) temperature (i.e., 150, 200, 250, 300, 350 and 400 °C for 5 h) and (b, d) time (i.e., 1, 2, 3, 4, 5, 6 and 7 h at 250 °C) of air oxidation.

on oxidized CTs were determined by the Boehm titration method. As shown in Fig. 2c, raising the oxidation temperature from 200 to 300 °C led to an increase of the concentration of total acidic groups from 1.1 to 3.3 mmol g^{-1}, whereas further temperature increases resulted in a reduction of the concentration of acidic groups (Fig. 2c). When the temperature was kept constant at 250 °C, the concentration of total acidic groups increased from 0.7 to 3.2 mmol g^{-1} as the time of oxidation increased from 1 to 7 h (Fig. 2d). These findings show that air oxidation at relatively mild temperatures can introduce acidic functional groups onto the surfaces of CTs, whereas oxidation at high temperatures results in their partial decomposition, confirming the findings from the pH studies (see Fig. 2a). Overall, air oxidation at temperatures of 250–300 °C for several hours appears to be favourable for the generation of acidic functional groups on CTs. Interestingly, the weak and moderate acidic groups are the main products formed on CTs during thermal air oxidation, whereas the strong acidic groups are only minor contributors. Generally, surface oxidation of carbonaceous materials is performed with strong mineral acids, such as nitric acid, which is a powerful oxidant and can produce a larger amount of strong acidic groups than oxidation by O_2 (air) (Rehman et al., 2019; Jaramillo et al., 2010). However, no studies are currently available that would suggest preferential NH_3/NH_4^+ adsorption on any specific types of acidic surface functional groups, and oxidation with aqueous oxidants possess the disadvantages of high maintenance cost and emission of secondary wastes. Using O_2 in air as oxidant provides a simple, environmentally friendly and non-hazardous alternative for the oxidative surface modification of carbonaceous materials.

The changes in surface functionality resulting from thermal air oxidation were further investigated using DRIFT and XPS. As shown in Fig. 3a, the DRIFT spectrum of the untreated CT revealed stretching vibrations at 3045 cm^{-1} (aromatic C–H) and at 2926 and 2855 cm^{-1} (aliphatic C–H), whereas the intensity of these signals decreased in the oxidized CT (CT-5-250 was exemplary analysed). Moreover, the intensity and relative peak area for the carbonyl (C═O) stretch of

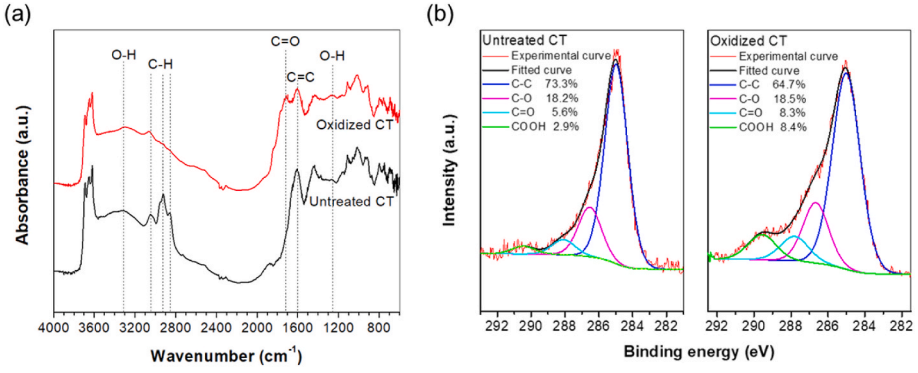

Fig. 3. Spectroscopic characterization of the untreated coal tailing (CT) and an exemplary CT sample exposed to thermal air oxidation (CT-5-250): (a) DRIFT spectra and (b) high-resolution XPS C 1s spectra. High-resolution XPS O 1s spectra are shown in Fig. S3 in the SI.

carboxylic acids at 1720 cm^{-1} increased remarkably after oxidation, in accordance with our previous observations for black coal (Zhang et al., 2020a). These findings suggested an oxidative transformation of aromatic and aliphatic C–H bonds into oxygen-containing functional groups during thermal oxidation. However, no significant changes were observed in the intensity of the broad band between 3200 and 3500 cm^{-1} caused by formation of phenolic or carboxylic O–H groups due to adsorbed water in the CTs. Furthermore, the incorporation of oxygen-containing functional groups during thermal air oxidation was confirmed by the XPS C 1s spectra, which revealed significant increases from 5.6 to 8.3% for carbonyl (C═O) and from 2.9 to 8.4% for carboxylic (COOH) groups (Fig. 3b). These findings are in line with the bulk elemental composition of the oxidized CT which has a greater O content (14.7%) compared with the untreated CT (8.7%, see Table 1).

3.3. NH_3 and NH_4^+ uptake

Compared with the untreated CT, the oxidized CTs showed an excellent NH_3 uptake. In particular, the CTs treated at 250 and 300 °C for 5 h achieved an NH_3 uptake of 45.3 and 52.5 mg g^{-1}, respectively (Fig. 4a). The result is similar or even exceeds the uptake capacity of previously described functionalized carbon materials (see Table S1 in the SI). Higher oxidation temperatures than 300 °C lowered the uptake capacity, which correlated with the observed partial decomposition and loss of acidic surface functional groups (see Fig. 2c). On the other hand, extending the oxidation time from 1 to 7 h, which was exemplary tested at 250 °C, resulted in a steady increase of the NH_3 uptake from 2.1 to 47.2 mg g^{-1} (Fig. 4b).

The oxidized CTs also showed an enhanced NH_4^+ uptake compared with the untreated material. Similar to NH_3, with increasing oxidation temperature the uptake of NH_4^+ by CTs increased, reaching a maximum removal efficiency of about 26% after treatment at 300 °C, but dropped at oxidation temperatures >300 °C (Fig. 4c). Likewise, increasing the oxidation time led to a continual increase of the NH_4^+ uptake (Fig. 4d), although the absolute uptake capacity for NH_4^+ was much lower than for NH_3. This finding could be rationalized by the acidic environment of oxidized CTs (see Fig. 2a and b), where the acidic functional groups responsible for NH_4^+ adsorption were only partially deprotonated (Sumaraj et al., 2020; Fidel et al., 2018; Wang et al., 2015). In addition, in the acidic aqueous NH_4Cl solution created by the oxidized CTs, H_3O^+ and soluble cations (e.g., K^+, Na^+, Mg^{2+} and Ca^{2+}) present in CTs may potentially compete with NH_4^+ for the same adsorption sites (Vu et al., 2017; Wang et al., 2015).

Overall, our data suggest that 300 °C is the optimum temperature for the oxidative surface modification of CTs with regards to capturing NH_3 and NH_4^+, where longer oxidation times improve uptake capacities. In the previous work, we have shown that lignite and oxidized black coal enable NH_3 uptake of 45.9–48.8 mg g^{-1} (which is similar to that of oxidized CTs shown here) can effectively reduce NH_3 volatilization form cattle manure by 36–44% (Zhang et al., 2022). Thus, considering the costs and energy consumption for thermal oxidation and the future applications of surface-modified CTs as agricultural amendments, treatment at 250–300 °C for 4–5 h appears to be a reasonable compromise for practical operation.

3.4. Role of surface functionalities on NH_3 uptake

The amount of NH_3 gas uptake by the oxidized CTs was linearly dependent on the concentration of total acidic groups, as indicated by a coefficient of determination (R^2) of 0.99 (Fig. 5a), whereas the R^2 values were slightly lower for the individual acidic groups (0.80, 0.89 and 0.91 for strong, moderate and weak acidic groups, respectively; see Fig. S4 in the SI). Obviously, all acidic functional groups on the oxidized CTs were involved in taking up NH_3. The slope of the linear relationship between the amount of NH_3 uptake and the concentration of total acidic groups, 0.85, is close to 1, indicating that NH_3 reacts with acidic groups in a 1:1 ratio on a molar basis, while the intercept of the linear regression (0.13) suggests that some level of physical adsorption also occur. On the other hand, a relatively weak relationship was found between the amount of NH_4^+ uptake from an aqueous solution and the concentration of acidic functional groups ($R^2 \leq 0.85$, see Fig. 5b and Fig. S4 in the SI), suggesting that NH_4^+ uptake was much less governed by the concentration of

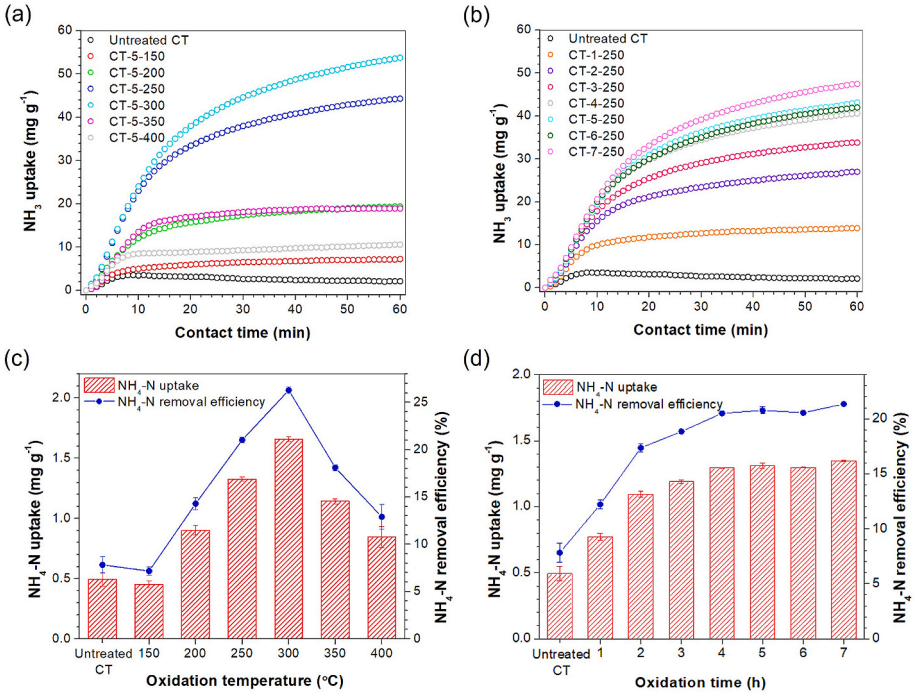

Fig. 4. Uptake of gaseous NH_3 (within 60 min) and NH_4^+ from an aqueous solution (after 24 h of equilibration) by the untreated and oxidized coal tailings (CTs): effect of (a, c) temperature (i.e., 150, 200, 250, 300, 350 and 400 °C for 5 h) and (b, d) time (i.e., 1, 2, 3, 4, 5, 6 and 7 h at 250 °C) of air oxidation. The NH_4^+ removal efficiency (blue lines) from an aqueous solution is also given in (c) and (d). Error bars represent the standard errors of triplicate experiments.

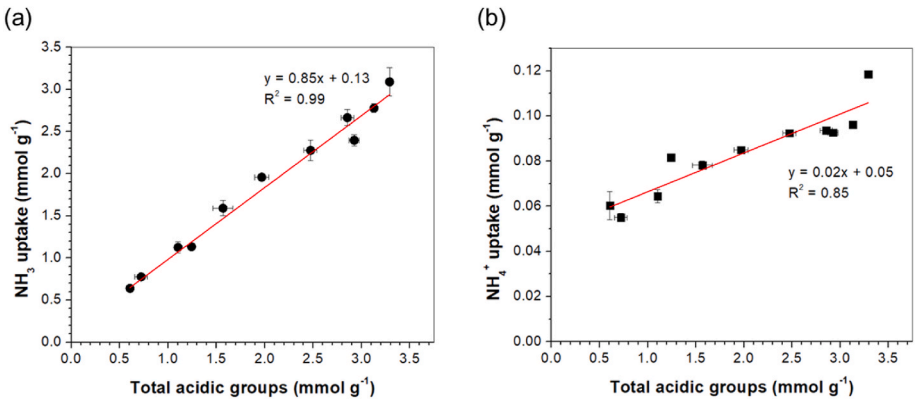

Fig. 5. (a) NH_3 and (b) NH_4^+ uptake by oxidized coal tailings as a function of total acidic functional groups.

acidic groups. These data suggest that at the pH of oxidized CTs the acidic groups are only partially deprotonated, which would reduce the amount of NH_4^+ held through electrostatic forces and which could be further exacerbated by competition with H_3O^+ and metal cations for the same adsorption sites, as discussed in the previous section.

The mechanism for the reaction of NH_3 with acidic functional groups was further investigated by analysing the untreated CT and an exemplary oxidized CT sample (CT-5-250) before and after exposure to NH_3 gas using DRIFT and XPS. Previous studies have proposed that NH_3 could be taken up by carboxylic groups on oxidized carbonaceous materials through an acid-base reaction (Fig. 6, pathway 1) and/or through nucleophilic addition, which leads to formation of amides with elimination of water (Fig. 6, pathway 2) (Goncalves et al., 2011; Seredych and Bandosz, 2007).

The DRIFT spectrum revealed that exposure of the oxidized CT to NH_3 (solid red curve) increased the absorption intensity in the 3200–3500 cm^{-1} region of O–H and N–H stretching vibrations (Mia et al., 2017; Petit, 2012; Goncalves et al., 2011), whereas similar changes were not observed in the untreated CT (solid black curve, Fig. 7a). Furthermore, for the oxidized CT the intensity of the C═O bands at 1720 cm^{-1} decreased compared with the spectrum obtained prior to NH_3 exposure, whereas the intensities of the bands in the 1600–1700 cm^{-1} region corresponding to the amide C═O considerably increased (Fig. 7b). An increase of the absorbance was also found for the amide N–H and C–N bands at 1557 cm^{-1}, suggesting that NH_3 can be retained on the oxidized CT surface through formation of amides (Goncalves et al., 2011; Seredych and Bandosz, 2007).

Analysis of the high-resolution XPS N 1s spectra of the CTs revealed three peaks with binding energies of 402.3–403.1 (corresponding to quaternary N, blue line), 400.2–400.8 (corresponding to pyrrolic N, pink line), and 398.2–399.4 eV (corresponding to pyridinic and amide N, green line, Fig. 7c and d). The relative proportions of each N species calculated from their peak areas for the untreated and oxidized CTs before and after exposure to NH_3 are summarized in Table 2. Thermal air

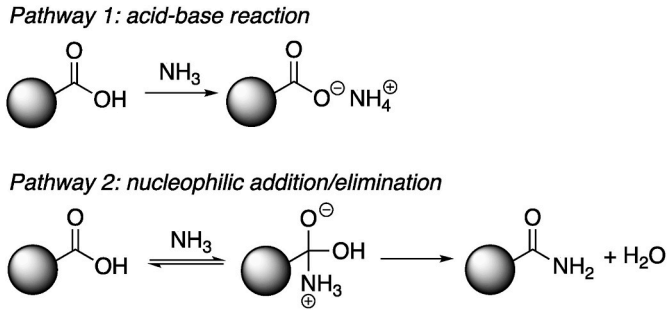

Fig. 6. Mechanism of NH_3 uptake by carboxylic groups on carbon surfaces (symbolized by the grey ball).

oxidation increased the proportion of quaternary N (55.8%) on CTs at the expense of pyrrolic N (33.3%) but without affecting pyridinic/amide N. The result may probably be ascribed to the protonation of pyridinic-N caused by adjacent or nearby located functional groups (e.g., hydroxyl, carboxyl and phenol) (Gong et al., 1999; Pels et al., 1995), and thermal degradation of pyrrolic-N (Phiri et al., 2017; Deng et al., 2013) and organic N (Gong et al., 1999).

Exposure to NH_3 gas resulted in an increase of the quaternary N peak for the untreated CT (from 46.3 to 55.1%) but not for the oxidized CT. In addition, the pyridinic/amide N proportion increased significantly from 10.9 to 20.1% when the oxidized CT was exposed to NH_3 gas, with the peak shifting to a higher binding energy of 399.4 eV, whereas the pyrrolic N decreased from 33.3 to 26.1%. The increased quaternary N sites in the untreated CT indicated NH_3 was captured by physical adsorption or as NH_4^+ species (Fig. 6, pathway 1), whereas the increase and shift to a higher binding energy in the pyridinic/amide N region in the case of the oxidized CT could be indicative for the formation of amide N through pathway 2 (see Fig. 6) (Krounbi et al., 2020; Wang et al., 2014; Petit, 2012). These results confirm the findings of DRIFT analysis that NH_3 can be retained on the oxidized CT surface through chemisorption as an amide.

It should be noted that the reaction of carboxylic acids with NH_3 to form amides is usually very slow at room temperature. We therefore suggest that this reaction could occur in microcracks formed during thermal oxidation of the CTs (Wang et al., 2022), where the high pressure caused by the surrounding material and the close proximity of the reaction partners in such a confined space are providing the driving force (Bandosz, 2021). On the other hand, the linear correlations between amount of NH_3 uptake and concentration of acidic functional groups (see Fig. 5a, Figure S4a,b and c) show that the weak and moderate acidic groups have also contributed to NH_3 uptake. However, the detection of such interactions may be impaired in spectroscopic analysis as the retention of NH_3 by weak and moderate acidic groups, such as hydroxyl groups, occurs through formation of hydrogen bonds (Petit, 2012). As these non-covalent interactions are relatively weak, the majority of H-bonded NH_3 could easily desorb from the adsorbent surface during analysis.

3.5. Kinetic analysis of the formation of acidic groups

The effect of oxidation temperature on the formation of acidic surface functional groups as a function of time was investigated at 200, 250 and 300 °C. As shown in Fig. 8a, the concentration of acidic groups on CTs increased continuously over the 7 h of exposure as the temperature of oxidation increased from 200 to 300 °C. The data were further analysed using the pseudo-first-order kinetic model (eq. (1)) since the oxidant (air) was present in large excess (Moore, 1972):

$$Q_t = Q_\infty\left(1 - e^{-kt}\right) \quad \text{(eq. 1)}$$

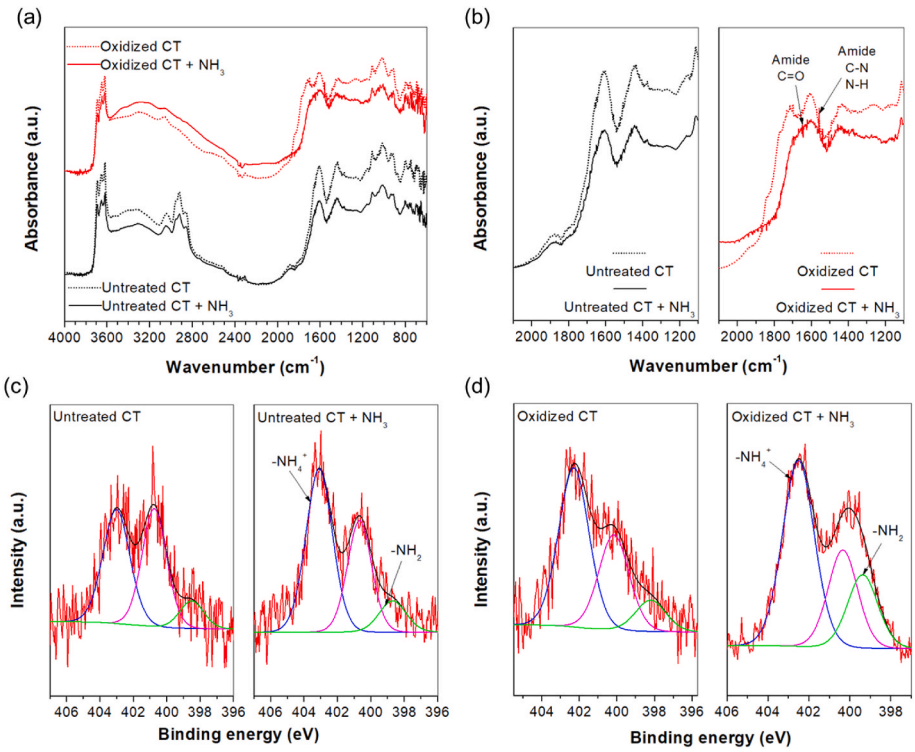

Fig. 7. Spectroscopic characterization of the untreated coal tailing (CT) and an exemplary oxidized CT sample (CT-5-250) before and after exposure to NH_3 gas: (a) DRIFT spectra; (b) DRIFT spectra in the energy range 2100–1100 cm^{-1}; (c) high-resolution XPS N 1s spectra for the untreated CT and (d) high-resolution XPS N 1s spectra for the oxidized CT.

Table 2
XPS N 1s binding energies and relative proportions of the three N species for the untreated coal tailing (CT) and an exemplary oxidized CT sample (CT-5-250) before and after exposure to NH_3 gas.

Sample	Binding energy (eV) and proportion			
	N 1s	Quaternary N	Pyrrolic N	Pyridinic/ Amide N
Untreated CT	400.0; 0.9%	403.0; 46.3%	400.8; 43.7%	398.5; 9.9%
Untreated CT + NH_3	400.0; 1.3%	403.1; 55.1%	400.7; 34.2%	398.7; 10.7%
Oxidized CT	401.0; 1.5%	402.3; 55.8%	400.2; 33.3%	398.2; 10.9%
Oxidized CT + NH_3	400.0; 1.9%	402.5; 53.8%	400.3; 26.1%	399.4; 20.1%

where Q_t (mmol g^{-1}) is the concentration of acidic groups per gram of sample generated at time t (h) determined by Boehm titration, Q_∞ (mmol g^{-1}) is the amount of acidic groups generated when time $t \rightarrow \infty$, and k (h^{-1}) is the pseudo-first-order rate coefficient. The formation of acidic groups on CTs fitted well with the pseudo-first-order kinetic model (the fitted lines are included in Fig. 8a), giving the rate coefficients of k = 0.06, 0.32 and 0.55 h^{-1} for 200, 250 and 300 °C, respectively. With these data, the activation energy (E_a) for the acidic group formation was obtained using the Arrhenius equation (eq. (2)):

$$\ln k = \ln A - \frac{E_a}{R}\frac{1}{T} \quad \text{(eq. 2)}$$

where A is the pre-exponential factor, R is the universal gas constant (8.314 J mol^{-1} K^{-1}), E_a (kJ mol^{-1}) is activation energy, and T (K) is the absolute temperature. The activation energy (E_a) of 50.2 kJ mol^{-1} for the acidic group formation on CTs was obtained using the slope of the

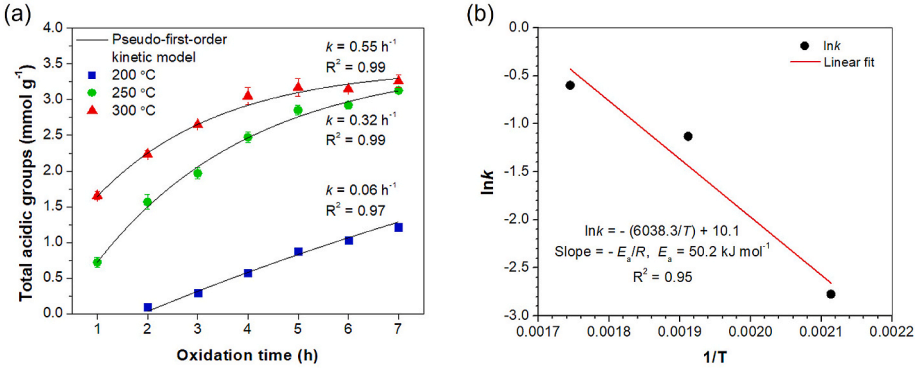

Fig. 8. (a) Effect of temperature (i.e., 200, 250 and 300 °C). on the formation of acidic groups on coal tailings and (b) Arrhenius plot to determine the activation energy (E_a) of acidic group formation in the range of 200–300 °C of oxidation.

line of the Arrhenius plot (Fig. 8b). To the best of our knowledge, this is the first time that the Arrhenius activation energy for the generation of surface functional group on carbonaceous materials has been determined.

In comparison with the activation energies for the thermal oxidation of aromatic compounds such as benzene and toluene (189.9 and 189.3 kJ mol^{-1}, respectively) (Everaert and Baeyens, 2004), the relatively low activation energy for acidic group formation on CTs determined here suggests a considerable amount of structural defects in the carbon framework of coals, which are prone to oxidation. Previous studies revealed a highly defective disordered structure of the carbon framework for coals by utilizing Raman spectroscopy (Nikitin et al., 2019; Song et al., 2019). Thus, formation of acidic groups on coal surfaces can occur with a low energy input, confirming that thermal air oxidation is a simple but effective method to surface modify carbonaceous materials for enhanced NH_3 uptake.

4. Conclusions

In this work we have demonstrated that coal tailings can be surface modified by thermal air oxidation to enable capture of NH_3 gas and NH_4^+ from an aqueous solution. Further analysis of the NH_3 capture process revealed a linear relationship ($R^2 = 0.99$) between NH_3 uptake and the concentration of total acidic surface functional groups that were formed during thermal oxidation of CTs. According to the data from the XPS and DRIFT analyses, carboxylic acid functional groups present on oxidized CT surfaces can capture NH_3 through formation of amides. Arrhenius plots revealed a remarkably low activation energy ($E_a = 50.2$ kJ mol^{-1}) for the formation of acidic functional groups on CTs during thermal air oxidation, clearly showing that thermal air oxidation is a simple and effective surface modification method to generate acidic surface functional groups on CTs to capture NH_3 gas. The abundance and ready availability of CTs and the comparably mild conditions and short reaction times required for surface modification of CTs make these materials promising candidates for mitigation of manure NH_3 emissions in livestock farms.

CRediT authorship contribution statement

Wei Zhang: Conceptualization, Methodology, Formal analysis, Investigation, Data curation, Writing – original draft, Visualization. **Bing Han:** Conceptualization, Methodology, Validation, Writing – review & editing. **Uta Wille:** Validation, Writing – review & editing. **Clayton Butterly:** Validation, Writing – review & editing. **Ji-Zheng He:** Validation, Writing – review & editing. **Deli Chen:** Conceptualization, Validation, Supervision, Writing – review & editing, Funding acquisition.

Declaration of competing interest

The authors declare that they have no known competing financial interests or personal relationships that could have appeared to influence the work reported in this paper.

Acknowledgment

This work was supported by the Australia-China Joint Research Centre "Healthy Soils for Sustainable Food Production and Environmental Quality" (ACSRF48165), the Victoria-Jiangsu Program for Technology and Innovation Research and Development (VIC-JS TECH) “Development of Novel Bio-Organic Fertilisers”, and the Melbourne Research Scholarship of The University of Melbourne. We thank Omid Mazaheri and the Trace Analysis for Chemical, Earth and Environmental Science (TrACEES) platform, The University of Melbourne for technical support.

Appendix A. Supplementary data

Supplementary data to this article can be found online at https://doi.org/10.1016/j.jclepro.2022.132525.

References

Bandosz, T.J., 2021. Exploring the silent aspect of carbon nanopores. Nanomaterials 11, 407. https://doi.org/10.3390/nano11020407.
Beusen, A.H.W., Bouwman, A.F., Heuberger, P.S.C., Van Drecht, G., Van Der Hoek, K.W., 2008. Bottom-up uncertainty estimates of global ammonia emissions from global agricultural production systems. Atmos. Environ. 42, 6067–6077. https://doi.org/10.1016/j.atmosenv.2008.03.044.
Bobrowski, A.B., Willink, D., Janke, D., Amon, T., Hagenkamp-Korth, F., Hasler, M., Hartung, E., 2021. Reduction of ammonia emissions by applying a urease inhibitor in naturally ventilated dairy barns. Biosyst. Eng. 204, 104–114. https://doi.org/10.1016/j.biosystemseng.2021.01.011.
Chen, D., Sun, J., Bai, M., Dassanayake, K.B., Denmead, O.T., Hill, J., 2015. A new cost-effective method to mitigate ammonia loss from intensive cattle feedlots: application of lignite. Sci. Rep. 5, 16689 https://doi.org/10.1038/srep16689.
Deng, L., Jin, X., Zhang, Y., Che, D., 2013. Release of nitrogen species during rapid pyrolysis of model coals. Energy Fuels 27, 430–439. https://doi.org/10.1021/ef3014053.
Edraki, M., Baumgartl, T., Manlapig, E., Bradshaw, D., Franks, D.M., Moran, C.J., 2014. Designing mine tailings for better environmental, social and economic outcomes: a review of alternative approaches. J. Clean. Prod. 84, 411–420. https://doi.org/10.1016/j.jclepro.2014.04.079.
Everaert, K., Baeyens, J., 2004. Catalytic combustion of volatile organic compounds. J. Hazard Mater. 109, 113–139. https://doi.org/10.1016/j.jhazmat.2004.03.019.
Fidel, R.B., Laird, D.A., Spokas, K.A., 2018. Sorption of ammonium and nitrate to biochars is electrostatic and pH-dependent. Sci. Rep. 8, 17627 https://doi.org/10.1038/s41598-018-35534-w.
Goertzen, S.L., Thériault, K.D., Oickle, A.M., Tarasuk, A.C., Andreas, H.A., 2010. Standardization of the Boehm titration. Part I. CO2 expulsion and endpoint determination. Carbon 48, 1252–1261. https://doi.org/10.1016/j.carbon.2009.11.050.
Goncalves, M., Sanchez-Garcia, L., Oliveira Jardim, E., Silvestre-Albero, J., Rodriguez-Reinoso, F., 2011. Ammonia removal using activated carbons: effect of the surface chemistry in dry and moist conditions. Environ. Sci. Technol. 45, 10605–10610. https://doi.org/10.1021/es203093v.
Gong, B., Buckley, A.N., Lamb, R.N., Nelson, P.F., 1999. XPS determination of the forms of nitrogen in coal pyrolysis chars. Surf. Interface Anal. 28, 126–130. https://doi.org/10.1002/(SICI)1096-9918, 28:1<126::AID-SIA633>3.0.CO;2-V, 199908.
Gu, B., Zhang, L., Dingenen, R.V., Vieno, M., Grinsven, H.J.V., Zhang, X., Zhang, S., Chen, Y., Wang, S., Ren, C., Rao, S., Holland, M., Winiwarter, W., Chen, D., Xu, J., Sutton, M.A., 2021. Abating ammonia is more cost-effective than nitrogen oxides for mitigating PM2.5 air pollution. Science 374, 758–762. https://doi.org/10.1126/science.abf8623.
Guffanti, P., Pifferi, V., Falciola, L., Ferrante, V., 2018. Analyses of odours from concentrated animal feeding operations: a review. Atmos. Environ. 175, 100–108. https://doi.org/10.1016/j.atmosenv.2017.12.007.
Hagenkamp-Korth, F., Haeussermann, A., Hartung, E., Reinhardt-Hanisch, A., 2015. Reduction of ammonia emissions from dairy manure using novel urease inhibitor formulations under laboratory conditions. Biosyst. Eng. 130, 43–51. https://doi.org/10.1016/j.biosystemseng.2014.12.002.
Han, B., Butterly, C., Zhang, W., He, J.-z., Chen, D., 2021. Adsorbent materials for ammonium and ammonia removal: a review. J. Clean. Prod. 283, 124611 https://doi.org/10.1016/j.jclepro.2020.124611.
Huang, C.-C., Li, H.-S., Chen, C.-H., 2008. Effect of surface acidic oxides of activated carbon on adsorption of ammonia. J. Hazard Mater. 159, 523–527. https://doi.org/10.1016/j.jhazmat.2008.02.051.
Jaramillo, J., Álvarez, P.M., Gómez-Serrano, V., 2010. Oxidation of activated carbon by dry and wet methods: surface chemistry and textural modifications. Fuel Process. Technol. 91, 1768–1775. https://doi.org/10.1016/j.fuproc.2010.07.018.
Krounbi, L., Enders, A., Anderton, C.R., Engelhard, M.H., Hestrin, R., Torres-Rojas, D., Dynes, J.J., Lehmann, J., 2020. Sequential ammonia and carbon dioxide adsorption on pyrolyzed biomass to recover waste stream nutrients. ACS Sustain. Chem. Eng. 8, 7121–7131. https://doi.org/10.1021/acssuschemeng.0c01427.
Le Leuch, L.M., Bandosz, T.J., 2007. The role of water and surface acidity on the reactive adsorption of ammonia on modified activated carbons. Carbon 45, 568–578. https://doi.org/10.1016/j.carbon.2006.10.016.
McIlroy, J.P., McGeough, K.L., Laughlin, R.J., Carolan, R., 2019. Abatement of ammonia emissions from dairy cow house concrete floor surfaces through additive application. Biosyst. Eng. 188, 320–330. https://doi.org/10.1016/j.biosystemseng.2019.10.016.
Mia, S., Dijkstra, F.A., Singh, B., 2017. Aging induced changes in biochar's functionality and adsorption behavior for phosphate and ammonium. Environ. Sci. Technol. 51, 8359–8367. https://doi.org/10.1021/acs.est.7b00647.
Mochizuki, T., Kubota, M., Matsuda, H., D'Elia Camacho, L.F., 2016. Adsorption behaviors of ammonia and hydrogen sulfide on activated carbon prepared from petroleum coke by KOH chemical activation. Fuel Process. Technol. 144, 164–169. https://doi.org/10.1016/j.fuproc.2015.12.012.
Moore, P., 1972. Analysis of kinetic data for a first-order reaction with unknown initial and final readings by the method of non-linear least squares. J. Chem. Soc., Faraday Trans. 1 (68), 1890–1893. https://doi.org/10.1039/F19726801890.

Nancharaiah, Y.V., Venkata Mohan, S., Lens, P.N.L., 2016. Recent advances in nutrient removal and recovery in biological and bioelectrochemical systems. Bioresour. Technol. 215, 173–185. https://doi.org/10.1016/j.biortech.2016.03.129.

Ng, E.L., Liang, X., Lam, S.K., Chen, D., Weatherley, A.J., 2020. What are the social costs and benefits of lignite application to reduce ammonia emissions in intensive feedlot? J. Environ. Manag. 269, 110821 https://doi.org/10.1016/j.jenvman.2020.110821.

Nikitin, A.P., Khabibulina, E.R., Mikhaylova, E.S., Zhuravleva, N.V., Ismagilov, Z.R., 2019. Structural defects and the demineralization of Kuznetsk basin coal: data from Raman spectroscopy. Coke Chem. 62, 169–173. https://doi.org/10.3103/S1068364X19050028.

Pels, J.R., Kapteijn, F., Moulijn, J.A., Zhu, Q., Thomas, K.M., 1995. Evolution of nitrogen functionalities in carbonaceous materials during pyrolysis. Carbon 33, 1641–1653. https://doi.org/10.1016/0008-6223(95)00154-6.

Petersen, S.O., 2018. Greenhouse gas emissions from liquid dairy manure: prediction and mitigation. J. Dairy Sci. 101, 6642–6654. https://doi.org/10.3168/jds.2017-13301.

Petit, C., 2012. Factors Affecting the Removal of Ammonia from Air on Carbonaceous Materials: Investigation of Reactive Adsorption Mechanism. Springer Science & Business Media, New York.

Phiri, Z., Everson, R.C., Neomagus, H.W.J.P., Wood, B.J., 2017. The effect of acid demineralising bituminous coals and de-ashing the respective chars on nitrogen functional forms. J. Anal. Appl. Pyrol. 125, 127–135. https://doi.org/10.1016/j.jaap.2017.04.009.

Radloff, B., Kirsten, M., Anderson, R., 2004. Wallerawang colliery rehabilitation: the coal tailings briquetting process. Miner. Eng. 17, 153–157. https://doi.org/10.1016/j.mineng.2003.10.023.

Rehman, A., Park, M., Park, S.-J., 2019. Current progress on the surface chemical modification of carbonaceous materials. Coatings 9. https://doi.org/10.3390/coatings9020103.

Santamarina, J.C., Torres-Cruz, L.A., Bachus, R.C., 2019. Why coal ash and tailings dam disasters occur. Science 364, 526. https://doi.org/10.1126/science.aax1927.

Seredych, M., Bandosz, T.J., 2007. Mechanism of ammonia retention on graphite oxides: role of surface chemistry and structure. J. Phys. Chem. C 111, 15596–15604. https://doi.org/10.1021/jp0735785.

Song, Y., Jiang, B., Qu, M., 2019. Macromolecular evolution and structural defects in tectonically deformed coals. Fuel 236, 1432–1445. https://doi.org/10.1016/j.fuel.2018.09.080.

Stokstad, E., 2014. Ammonia pollution from farming may exact hefty health costs. Science 343, 238. https://doi.org/10.1126/science.343.6168.238.

Sumaraj, Xiong, Z., Sarmah, A.K., Padhye, L.P., 2020. Acidic surface functional groups control chemisorption of ammonium onto carbon materials in aqueous media. Sci. Total Environ. 698, 134193 https://doi.org/10.1016/j.scitotenv.2019.134193.

Sun, J., Bai, M., Shen, J., Griffith, D.W.T., Denmead, O.T., Hill, J., Lam, S.K., Mosier, A. R., Chen, D., 2016. Effects of lignite application on ammonia and nitrous oxide emissions from cattle pens. Sci. Total Environ. 565, 148–154. https://doi.org/10.1016/j.scitotenv.2016.04.156.

Sutton, M.A., Oenema, O., Erisman, J.W., Leip, A., van Grinsven, H., Winiwarter, W., 2011. Too much of a good thing. Nature 472, 159–161. https://doi.org/10.1038/472159a.

Tremain, P., Zanganeh, J., Hugo, L., Curry, S., Moghtaderi, B., 2014. Characterization of "chailings": a char created from coal tailings. Energy Fuel. 28, 7609–7615. https://doi.org/10.1021/ef501829f.

Vivo-Vilches, J.F., Bailón-García, E., Pérez-Cadenas, A.F., Carrasco-Marín, F., Maldonado-Hódar, F.J., 2014. Tailoring the surface chemistry and porosity of activated carbons: evidence of reorganization and mobility of oxygenated surface groups. Carbon 68, 520–530. https://doi.org/10.1016/j.carbon.2013.11.030.

Vu, T.M., Trinh, V.T., Doan, D.P., Van, H.T., Nguyen, T.V., Vigneswaran, S., Ngo, H.H., 2017. Removing ammonium from water using modified corncob-biochar. Sci. Total Environ. 579, 612–619. https://doi.org/10.1016/j.scitotenv.2016.11.050.

Wang, B., Lehmann, J., Hanley, K., Hestrin, R., Enders, A., 2015. Adsorption and desorption of ammonium by maple wood biochar as a function of oxidation and pH. Chemosphere 138, 120–126. https://doi.org/10.1016/j.chemosphere.2015.05.062.

Wang, D.H., Hu, Y., Zhao, J.J., Zeng, L.L., Tao, X.M., Chen, W., 2014. Holey reduced graphene oxide nanosheets for high performance room temperature gas sensing. J. Mater. Chem. 2, 17415–17420. https://doi.org/10.1039/C4TA03740E.

Wang, H., Dlugogorski, B.Z., Kennedy, E.M., 2003. Coal oxidation at low temperatures: oxygen consumption, oxidation products, reaction mechanism and kinetic modelling. Prog. Energ. Combust. 29, 487–513. https://doi.org/10.1016/s0360-1285(03)00042-x.

Wang, J.Z., Hu, Z.Y., Zhou, X.Q., An, Z.Z., Gao, J.F., Liu, X.N., Jiang, L.L., Lu, J., Kang, X. M., Li, M., Hao, Y.B., Kardol, P., 2012. Effects of reed straw, zeolite, and superphosphate amendments on ammonia and greenhouse gas emissions from stored duck manure. J. Environ. Qual. 41, 1221–1227. https://doi.org/10.2134/jeq2011.0373.

Wang, X., Ma, H., Qi, X., Gao, K., Li, S., Yang, X., 2022. Experimental study on the effect of high-temperature oxidation coal mechanical characteristics. PLoS One 17, e0264039. https://doi.org/10.1371/journal.pone.0264039.

Xu, R., Tian, H., Pan, S., Prior, S.A., Feng, Y., Batchelor, W.D., Chen, J., Yang, J., 2019. Global ammonia emissions from synthetic nitrogen fertilizer applications in agricultural systems: empirical and process-based estimates and uncertainty. Global Change Biol. 25, 314–326. https://doi.org/10.1111/gcb.14499.

Zhang, W., Butterly, C., Han, B., He, J.-Z., Chen, D., 2022. Modified lignite and black coal reduce ammonia volatilization from cattle manure. J. Environ. Manag. 301, 113807 https://doi.org/10.1016/j.jenvman.2021.113807.

Zhang, W., Han, B., He, J.-Z., Chen, D., 2020a. Modification of bituminous coal by air oxidation to increase ammonia capture. J. Anal. Appl. Pyrol. 151, 104930 https://doi.org/10.1016/j.jaap.2020.104930.

Zhang, X., Gu, B., van Grinsven, H., Lam, S.K., Liang, X., Bai, M., Chen, D., 2020b. Societal benefits of halving agricultural ammonia emissions in China far exceed the abatement costs. Nat. Commun. 11, 4357. https://doi.org/10.1038/s41467-020-18196-z.

Zhang, Y., Li, Y., Huang, Y., Li, S., Wang, W., 2017. Characteristics of mass, heat and gaseous products during coal spontaneous combustion using TG/DSC–FTIR Technology. J. Therm. Anal. Calorim. 131, 2963–2974. https://doi.org/10.1007/s10973-017-6738-x.

Zheng, W., Hu, J., Rappeport, S., Zheng, Z., Wang, Z., Han, Z., Langer, J., Economy, J., 2016. Activated carbon fiber composites for gas phase Ammonia adsorption. Microporous Mesoporous Mater. 234, 146–154. https://doi.org/10.1016/j.micromeso.2016.07.011.